JOURNAL OF COMPUTATIONAL PHYSICS 72, 435–448 (1987)

Some Practical Considerations Involving Spectral Representations of 3D Plasma Equilibria*

S. E. ATTENBERGER

Computing and Telecommunications Division, Oak Ridge National Laboratory, Oak Ridge, Tennessee 37831

AND

W. A. HOULBERG AND S. P. HIRSHMAN

Fusion Energy Division, Oak Ridge National Laboratory, Oak Ridge, Tennessee 37831

Received July 29, 1986; revised January 9, 1987

For describing magnetically confined toroidal plasmas, it is convenient in some instances to use a cylindrical coordinate system whose origin is on the major axis of the torus and in others to use a "flux coordinate" system bound to the magnetic flux which is embedded in the plasma. A good estimate of the flux surface geometry is available in spectral form in many cases, permitting a simple transformation from flux coordinates to cylindrical coordinates. A modified Newton iteration is described for performing the "inverse" transformation from cylindrical coordinates to flux coordinates. An accurate technique for radial spline interpolation of the spectral coefficients is given which is particularly useful for computing magnetic fields near the magnetic axis. Given a spectral representation of the plasma it is possible to track a chord through the plasma, determining in sequence its intersections with a given set of flux surfaces. This technique is the starting point for many calculations including neutral beam heating, pellet fueling, evaluation of absorption or plasma sources along the lines-of-sight of detectors, etc. An efficient algorithm for performing this calculation is given. These algorithms permit the determination of plasma "profiles" from chordal data by a straightforward least-squares technique, without any restrictions on the orientation of the chords. The method shown is contrasted to those based on generalized Abel transforms.

1. INTRODUCTION

Let (R, ϕ, Z) be a cylindrical coordinate system whose origin is on the major axis of a magnetically confined toroidal plasma. (R is the major radius, ϕ is the toroidal

* Research sponsored by the Office of Fusion Energy, U. S. Department of Energy, under Contract DE-AC05-84OR21400 with Martin Marietta Energy Systems, Inc. The U.S. Government's right to retain a nonexclusive royalty-free license in and to the copyright covering this paper, for governmental purposes, is acknowledged.

581/72/2-11

0021-9991/87 $3.00

angle, and Z is the distance above the midplane.) To relate flux surface quantities such as plasma density, temperature, etc., to cylindrical coordinates, we must also have another coordinate system, one that is embedded in the plasma. For convenience, we define the "flux coordinates" [1–4] (ρ, θ, ζ) as follows: θ is a poloidal coordinate, ζ is a toroidal coordinate, and ρ is a radial coordinate labeling a flux surface defined by $\mathbf{B} \cdot \nabla \rho = 0$, where $\mathbf{B}$ is the magnetic field. Let

$$R(\rho, \theta, \zeta) = \sum_m \sum_n R_{mn}(\rho) \cos(m\theta - n\zeta), \tag{1a}$$

$$Z(\rho, \theta, \zeta) = \sum_m \sum_n Z_{mn}(\rho) \sin(m\theta - n\zeta), \tag{1b}$$

$$\phi(\rho, \theta, \zeta) = \zeta. \tag{1c}$$

Equations (1a) and (1b) are appropriate for plasmas that have vertical symmetry in at least two toroidal planes per field period (stellarator symmetry). This restriction, as well as the restriction that $\zeta = \phi$, could be relaxed by extending the following analysis in a straightforward way.

In Section 2, we describe an iterative technique for the "inverse" transformation from (R, ϕ, Z) to (ρ, θ, ζ). We have chosen $\zeta = \phi$ for computational convenience. Particular definitions of ρ and θ, which relate the flux coordinates to the magnetic field, are given in Sections 2 and 3, respectively.

The coefficients of the transformation (sometimes called "spectral coefficients") are generally given at a discrete set of ρ values by a magnetohydrodynamic equilibrium code or by a vacuum field line following algorithm. Splines can be used to interpolate the data in the ρ direction; special care is needed, however, in interpolating the data near the magnetic axis, particularly when computing the magnetic field. We show a way to reduce interpolation errors near the magnetic axis. In some cases, such as tracing rays that leave and reenter the plasma, extending the transformation beyond the plasma is useful. Because simple extrapolation of the splines works very poorly, a more robust (but still arbitrary) continuation of the transformation is given in Section 2. Section 3 lists the equations for the magnetic field in terms of the parameters chosen here and shows an example of errors in the field due to an inferior spline fit.

In Section 4 an efficient algorithm is described for finding, in sequence, the intersections of a straight trajectory with a set of nested flux surfaces. This algorithm builds on the techniques of Section 2 and forms the starting point for Section 5, which shows how plasma profiles may be determined from chordal data when the spectral coefficients are known.

2. The "Inverse" Transformation

Given R, Z, and ϕ, we wish to compute the values of ρ and θ. Taylor-expanding R and Z about the approximate solution (ρ^k, θ^k) yields

$$R(\rho, \theta) = R^k + R^k_\theta(\theta - \theta^k) + R^k_\rho(\rho - \rho^k) + \cdots, \tag{2a}$$

$$Z(\rho, \theta) = Z^k + Z^k_\theta(\theta - \theta^k) + Z^k_\rho(\rho - \rho^k) + \cdots, \tag{2b}$$

where subscripts denote derivatives and where R^k and Z^k are the values obtained by evaluating Eqs. (1a) and (1b) at ρ^k and θ^k. Neglecting terms involving second and higher derivatives, we can solve Eqs. (2a) and (2b) simultaneously for ρ and θ at the $(k+1)$th iteration. The solution is

$$\theta^{k+1} = \theta^k + \frac{Z^k_\rho(R - R^k) - R^k_\rho(Z - Z^k)}{\tau^k}, \tag{3a}$$

$$\rho^{k+1} = \rho^k + \frac{R^k_\theta(Z - Z^k) - Z^k_\theta(R - R^k)}{\tau^k}, \tag{3b}$$

where

$$\tau = R_\theta Z_\rho - R_\rho Z_\theta \tag{4}$$

is the Jacobian of the transformation from (R, Z) to (ρ, θ). Note that derivatives with respect to θ and ζ are available trivially from Eqs. (1a) and (1b), but derivatives with respect to ρ must typically be derived from spline fits of the $R_{mn}(\rho)$ and $Z_{mn}(\rho)$. This algorithm typically converges in two to six iterations with the error $|R^k - R|/R$ decreasing by about an order of magnitude per iteration. A poor initial guess costs only a couple of iterations in most cases. Convergence is said to be achieved when $(R^k - R)^2 + (Z^k - Z)^2 < \varepsilon_I$, where ε_I is a small distance.

In pathological cases the $(k+1)$th iteration may give a worse result than the kth iteration. In that case the step size is halved, and an estimated mean value is used for the Jacobian as follows:

$$\theta^{k+2} = \theta^k + \frac{1}{2}\frac{Z^k_\rho(R - R^k) - R^k_\rho(Z - Z^k)}{0.75\tau^k + 0.25\tau^{k+1}}, \tag{5a}$$

$$\rho^{k+2} = \rho^k + \frac{1}{2}\frac{R^k_\theta(Z - Z^k) - Z^k_\theta(R - R^k)}{0.75\tau^k + 0.25\tau^{k+1}}. \tag{5b}$$

If necessary, the reduced step can be reduced again in a similar fashion. We have not observed any cases that fail to converge when treated in this way. Of course the problem could also be solved by using a library routine to find the zero of a function such as $F(\rho^k, \theta^k) = (R - R^k)^2 + (Z - Z^k)^2$. This is appropriate if a code must be constructed quickly. However, for production work the method presented

here is fast, robust, and straightforward. It has no unnecessary overhead and requires no adjustments to achieve optimal convergence.

Regardless of the iterative procedure used, special care is needed near the magnetic axis. To be specific, we must pick a definition of ρ. We let

$$\rho = (\Phi/\Phi_a)^{1/2}, \tag{6}$$

where Φ is the toroidal magnetic flux contained within a flux surface and Φ_a is the value of Φ at the plasma boundary. Then τ approaches zero at the magnetic axis and the transformation is undefined. If $\rho^k = 0$ but $(R^k, Z^k) \neq (R, Z)$, then we set $\rho^k = \rho_{\min}$ in order to proceed. Typically, $\rho_{\min}$ is taken as ten times machine precision.

A related problem is that the quantities Z_ρ and R_ρ must be determined very accurately in the region where ρ is small to ensure a nonzero value for τ. It can be shown [1] that the $R_{mn}(\rho)$ and $Z_{mn}(\rho)$ are proportional to ρ^m as ρ approaches zero. To interpolate the data accurately, we factor out the dependence on ρ^m prior to performing the spline fit in ρ. We let

$$R(\rho, \theta, \zeta) = \sum_m \sum_n \rho^m \tilde{R}_{mn}(\rho) \cos(m\theta - n\zeta) \tag{7a}$$

and

$$Z(\rho, \theta, \zeta) = \sum_m \sum_n \rho^m \tilde{Z}_{mn}(\rho) \sin(m\theta - n\zeta), \tag{7b}$$

where the quantities $\tilde{R}_{mn}(\rho)$ and $\tilde{Z}_{mn}(\rho)$ are the fitted functions. This form is particularly useful if the data are rather sparse near the axis. We will return to this point in the next section. Note that if data is not available at $\rho = 0$, a reasonable extrapolation from neighboring data points may be made using the ρ^m behavior.

In many practical applications, extending the transformation given by Eqs. (1a) and (1b) beyond the plasma is useful, even though the identification of ρ with magnetic flux surfaces may be meaningless for $\rho > 1$. A simple extension which gives a unique mapping for plasma boundaries which are not too severely concave is obtained as follows: let R_{10} and Z_{10} be proportional to ρ, and all other coefficients be constant for $\rho \geqslant 1$. This causes the flux surfaces to approach ellipses as $\rho \to \infty$. Note that a discontinuity in τ occurs at $\rho = 1$ using this algorithm. Equations (5a) and (5b) are very effective in dealing with a discontinuity in τ. Other treatments are possible. In particular, τ could be made continuous by causing the R_{mn} and Z_{mn} to be smooth functions of ρ. However, for applications such as tracking a chord to determine its intersections with a plasma (see Section 4), the computation of the additional spectral coefficients for $\rho > 1$ would slow down the calculation without increasing the accuracy.

3. Magnetic Field Calculation

The magnetic field associated with the flux coordinates (ρ, θ, ζ) can be written as [5, 6]

$$\mathbf{B} = \frac{\nabla \Phi}{2\pi} \times (\nabla \theta^* - \iota \nabla \zeta), \tag{8}$$

where Φ is the toroidal magnetic flux, $\iota = \Psi'/\Phi'$, Ψ is the poloidal magnetic flux, primes denote derivatives with respect to ρ, and θ^* is the poloidal angle that makes the field lines "straight." To reduce the number of modes required to describe the transformation, we introduce the parameter λ, which satisfies

$$\theta^* = \theta + \lambda(\rho, \theta, \zeta), \tag{9}$$

where λ may be represented as

$$\lambda(\rho, \theta, \zeta) = \sum_m \sum_n \rho^m \tilde{\lambda}_{mn}(\rho) \sin(m\theta - n\zeta) \tag{10}$$

and the coefficients of the expansion are determined along with those for R and Z by a steepest descent method [1]. The following discussion may of course be applied to straight field line coordinates by setting $\lambda = \lambda_\theta = \lambda_\zeta = 0$. Equation (10) is appropriate for plasmas that have stellarator symmetry.

It can be shown that

$$\mathbf{B} = \frac{\Phi'}{2\pi R\tau} [(\iota - \lambda_\zeta)\mathbf{e}_\theta + (1 + \lambda_\theta)\mathbf{e}_\zeta], \tag{11}$$

where $\mathbf{e}_\theta \equiv \partial \mathbf{x}/\partial\theta$ and $\mathbf{e}_\zeta \equiv \partial \mathbf{x}/\partial\zeta$ are covariant basis vectors. Given values for ρ and θ and assuming that Φ_a and $\iota(\rho)$ are known, we can solve for the magnetic field components using Eqs. (1a), (1b), (4), (6), (10), and (11). For convenience we list expressions for the cylindrical components of **B**.

$$B^R = \frac{\Phi'}{2\pi R\tau} [(\iota - \lambda_\phi) R_\theta + 1(1 + \lambda_\theta) R_\phi] \tag{12}$$

$$B^Z = \frac{\Phi'}{2\pi R\tau} [(\iota - \lambda_\phi) Z_\theta + (1 + \lambda_\theta) Z_\phi] \tag{13}$$

$$B_{\text{tor}} = \frac{\Phi'}{2\pi\tau}(1 + \lambda_\theta). \tag{14}$$

Note that Φ' and τ both approach zero as $\rho \to$ zero, so accurate determination of τ near the magnetic axis is critical in order to get sensible values for **B**. Small errors in the R_{mn} and Z_{mn} data can cause large errors in the resulting **B** values near the

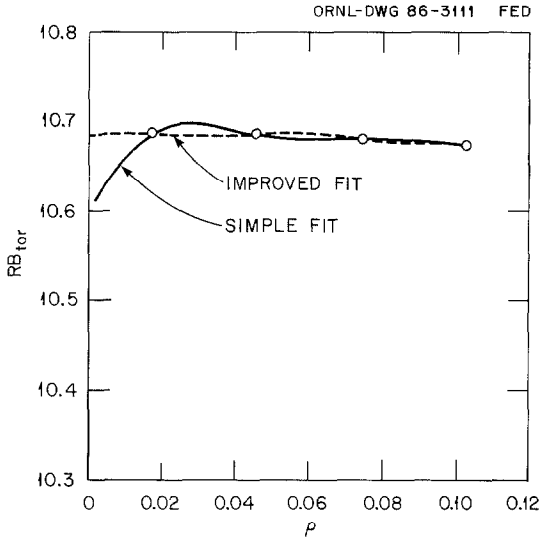

FIG. 1. Factoring out ρ^m prior to spline fitting the spectral coefficients improves the calculated value of the magnetic field near $\rho = 0$.

axis, and thus careful determination of the equilibrium is required if the magnetic field is to be reconstructed in this way. Figure 1 shows the importance of factoring out the ρ^m dependence prior to spline fitting the Fourier coefficients. For a typical tokamak geometry the flux surface quantity RB_{tor} (major radius times toroidal magnetic field) is plotted versus ρ near the magnetic axis. The solid line results from spline fitting the R_{mn}, Z_{mn}, and λ_{mn} coefficients. The dashed line corresponds to factoring out ρ^m prior to the spline fits. The open circles label RB_{tor} values corresponding to the knots of the splines. (In addition there is a knot at $\rho = 0$, where the expression for B_{tor} is indeterminate.)

The magnetic field calculation described here has been used in numerical calculation of stellarator transport coefficients from the linearized drift

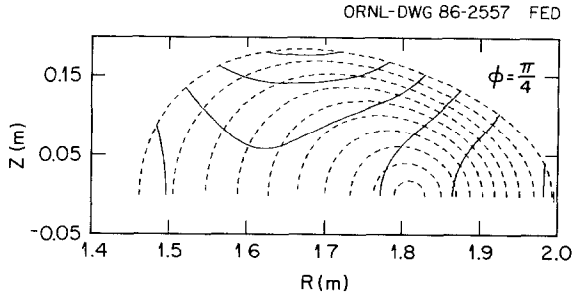

FIG. 2. Mod(**B**) contours.

Fokker–Planck equation, using equilibria generated by the 3D MHD equilibrium codes MOMCON and VMEC [9, 10]. Figure 2 shows mod(**B**) contours for the $\phi = \pi/4$ plane of the Advanced Toroidal Facility (ATF). The data for $R_{mn}(\rho)$, $Z_{mn}(\rho)$, $\lambda_{mn}(\rho)$, and $\iota(\rho)$ were available on a 31-point grid, uniformly spaced in ρ. An arbitrary set of flux surfaces (uniformly spaced in ρ) is shown by the dashed curves.

4. Tracking a Chord

Suppose that we wish to find all the intersections of a straight trajectory with a given set of flux surfaces. Furthermore, they should be in the order that they would be encountered when traveling along the trajectory. This is useful for such applications as neutral beam heating of plasmas. The fundamental technique is to take a step along the trajectory in such a way as to cross one and only one flux surface. Then the intersection with that flux surface corresponds to the zero of the function $\rho(S) - \rho_i$ on the interval (S^k, S^{k+1}), where S is the path length along the trajectory, ρ_i is the ρ value of the flux surface crossed, S^k is the start of the step, and S^{k+1} is the end of the step.

It may be shown that the variation of ρ along the trajectory satisfies

$$\rho'(S) \equiv \frac{\partial \rho}{\partial S} = \left[\frac{\partial \rho}{\partial R}\left(\frac{X}{R}\right) + \frac{\partial \rho}{\partial \phi}\left(-\frac{Y}{R^2}\right)\right]\frac{\partial X}{\partial S} + \left[\frac{\partial \rho}{\partial R}\left(\frac{Y}{R}\right) + \frac{\partial \rho}{\partial \phi}\left(\frac{X}{R^2}\right)\right]\frac{\partial Y}{\partial S} + \frac{\partial \rho}{\partial Z}\frac{\partial Z}{\partial S}, \tag{15}$$

where S is path length along the trajectory and $(X = R\cos\phi,\ Y = R\sin\phi, Z)$ are Cartesian coordinates. Since the trajectory is straight in real space, the quantities $\partial X/\partial S$, $\partial Y/\partial S$, and $\partial Z/\partial S$ are constants along the trajectory. The remaining derivatives depend on the local Jacobian, i.e.,

$$\frac{\partial \rho}{\partial R} = \frac{1}{\tau}\left(-\frac{\partial Z}{\partial \theta}\right) \tag{16}$$

$$\frac{\partial \rho}{\partial \phi} = \frac{1}{\tau}\left(\frac{\partial R}{\partial \phi}\frac{\partial Z}{\partial \theta} - \frac{\partial R}{\partial \theta}\frac{\partial Z}{\partial \phi}\right) \tag{17}$$

$$\frac{\partial \rho}{\partial Z} = \frac{1}{\tau}\left(\frac{\partial R}{\partial \theta}\right). \tag{18}$$

Suppose that the plasma is divided into nested volume elements whose boundaries ρ_i are flux surfaces, where $0 \leqslant \rho_i \leqslant 1$. In addition, a dummy volume element $1 < \rho \leqslant \rho_{\max}$ is defined to permit treatment of trajectories which lie outside of the plasma. At any point S^k on the trajectory one may determine $\rho^k \equiv \rho(S^k)$ and find

which volume element S^k lies in. Suppose that the surface ρ_i forms one of the boundaries of the current volume element. Then the path length to ρ_i is approximately

$$\Delta S_i^k = (\rho_i - \rho^k)/\rho'(S^k). \tag{19}$$

Let ρ_i be the surface which makes $\Delta S_i^k > 0$; then we attempt to span the intersection with ρ_i by taking a step $\Delta S^k = 1.1\,\Delta S_i^k$. Several tests are then performed to see whether one and only one surface has been spanned.

If $\rho^{k+1} = \rho(S^k + \Delta S^k)$ does not lie in the same volume element or an adjacent element, the step size is halved. However, the step size is required to be at least ε_S, where the choice of ε_S is discussed later.

If $\Delta S^k > L_{\max}$ or $\Delta S^k > S_{\max}$ the step is truncated, where $S_{\max}$ is the length of the trajectory and $L_{\max}$ is chosen so that $\rho'(S)$ changes sign no more than once per step. Normally $L_{\max}$ can be set equal to the minor radius, but in highly rippled plasmas it should be set less than the ripple spacing. Note that a change of sign in $\rho'(S)$ indicates that the trajectory is tangent to some surface ρ_T, which may or may not coincide with one of the ρ_i.

If $\rho'(S^{k+1})$ has the opposite sign of $\rho'(S^k)$, then we find the zero of the function $\rho'(S)$ on the interval (S^k, S^{k+1}) using the ZEROIN routine in a form similar to that presented by Forsythe *et al.* [11]. The step is shortened to fall at the solution point S_T, avoiding the possibility of missing a tangency point or a closely spaced pair of intersections when $\rho_T \approx \rho_i$.

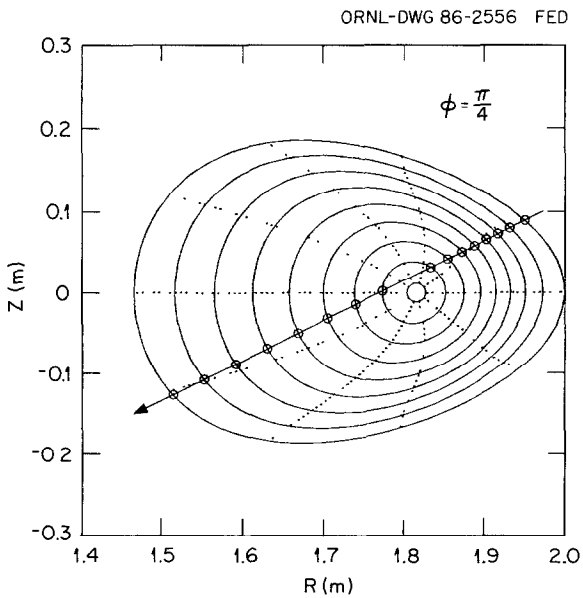

FIG. 3. Intersections of a straight line lying in a ϕ = constant plane with a set of flux surfaces.

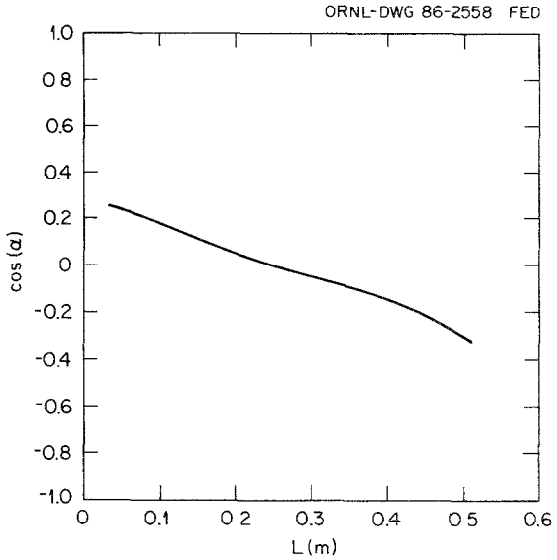

FIG. 4. Cos α vs path length along the trajectory.

If $\rho'(S)$ does not change sign but the step falls short of the surface ρ_l, then we set $S^k = S^{k+1}$ and recompute ΔS_l^k.

If none of the above conditions are met, then the step spans one and only one surface and we find the intersection $\rho(S) - \rho_l = 0$ on the interval (S^k, S^{k+1}) using ZEROIN.

The ZEROIN procedure is required to converge within some tolerance $\Delta S < \varepsilon_Z$. After an intersection or a zero of $\rho'(S)$ has been found at some point S_Z we check the sign of $\rho'(S_Z + \varepsilon_S)$ in order to find which surface the trajectory will approach next, and the procedure is repeated. The minimum step ε_S is necessary after an intersection in order to prevent finding the same intersection again when $S_i > S_Z \geqslant S_i - \varepsilon_Z$, where S_i is the exact position of the intersection. It is critical to maintain the relation $\varepsilon_S > \varepsilon_Z > \varepsilon_I$ among the minimum step size, the ZEROIN tolerance, and the inverse transformation tolerance, respectively. A reasonable choice is $\varepsilon_S = 2\varepsilon_Z = 200\varepsilon_I = L_{\max}/100$. (Note that $\rho(S)$ and $\rho'(S)$ must be obtained using a sequence of transformations $(X(S), Y(S), Z(S)) \to (R(S), Z(S), \phi(S)) \to (\rho(S), \theta(S), \phi(S))$, where the last transformation is the inverse transformation described in Section 2).

Figure 3 shows the intersections of a set of nested flux surfaces with a trajectory in the $\phi = \pi/4$ plane of the ATF. The dotted lines are surfaces of constant θ. This case took less than 0.005s of execution time per intersection on the CRAY-I for an equilibrium described by nine spectral modes. (See Eqs. (1a) and (1b).) This is typical for any trajectory (including trajectories that do not lie in a $\phi =$ constant plane), with execution time being roughly proportional to the number of modes.

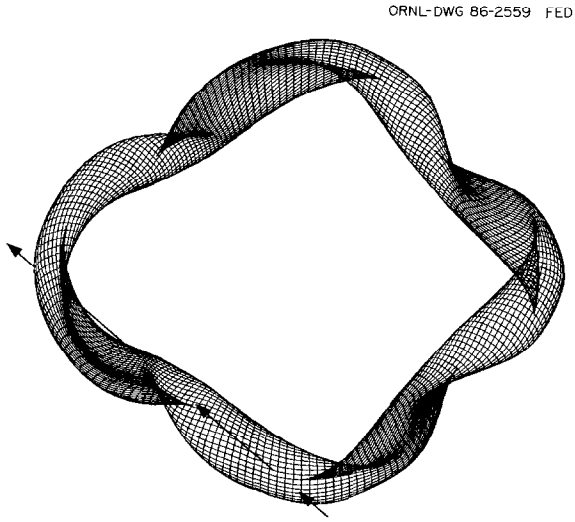

FIG. 5. Trajectory intersecting Heliac plasma multiple times (perspective view). The arrows show those parts of the trajectory which lie outside the plasma. The second arrow lies on the opposite side of the plasma from the viewer.

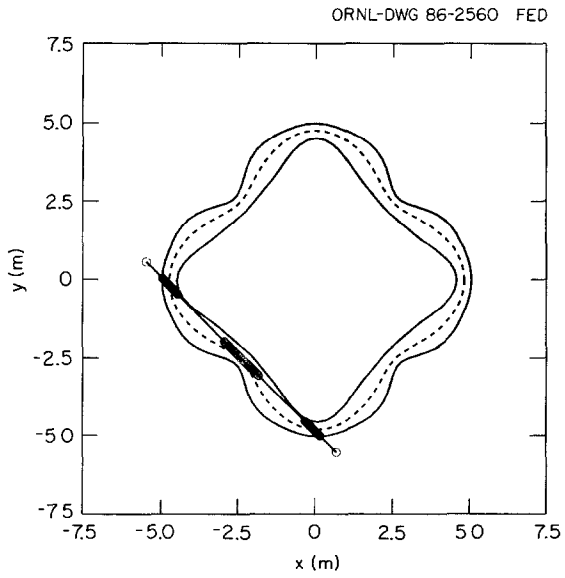

FIG. 6. Trajectory intersecting Heliac plasma multiple times (top view). The small circles indicate the ends of the trajectory and the intersections of the trajectory with a set of nested flux surfaces (not shown).

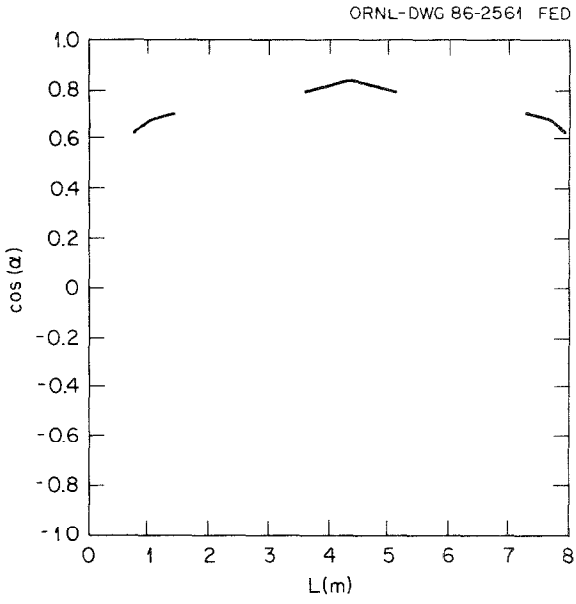

FIG. 7. Cos α vs path length along the trajectory

In the modeling of neutral beam injection, it is useful to know the value of α, the angle between the particle trajectory and the magnetic field. Note that

$$\cos \alpha = \frac{\mathbf{L} \cdot \mathbf{B}}{|\mathbf{L}|\,|\mathbf{B}|}, \tag{20}$$

where **L** is a path-length vector along the trajectory. This expression is most easily evaluated by converting the cylindrical components of **B** (Eqs. (12)–(14)) to the corresponding Cartesian components. Figure 4 shows cos α as a function of path length for the trajectory in Fig. 3.

To illustrate the power of this technique, we consider a trajectory that intersects a heliac plasma several times. Figure 5 shows a perspective view. It is helpful to compare it with Fig. 6, which shows a top view of the trajectory with the outline of the plasma and the magnetic axis. Figure 7 shows cos α as a function of path length for this trajectory. Note that cos α is not computed for those portions of the trajectory which lie outside of the plasma, since our data come from a fixed-boundary equilibrium code which does not model the magnetic field for $\rho > 1$.

5. CHORDAL DATA INVERSION

In a magnetically confined toroidal plasma, quantities such as density and temperature are nearly constant on a flux surface. Plots of these quantities as a function

of ρ are called "profiles." A problem frequently encountered in experimental plasma physics is that of finding a plasma profile given measurements of absorption or source strength along a set of chords which are the lines of sight of an array of detectors. The measured values may be expressed as line integrals of some quantity which is constant on a flux surface. If the spectral coefficients in Eq. (1a) and (1b) are known, the profiles may be determined by a straightforward least-squares method. Note that this is not the same as "Abel inversion" or the more general tomographic analysis of Granetz and Camacho [7], which do not assume any knowledge of flux surface shapes and which require the chords to lie in a plane at one toroidal position.

For example, suppose we want to know the bremsstrahlung source strength as a function of ρ. The experimental data are a set of photon counting rates from an array of collimated detectors. If S_k is the signal from the kth detector, then

$$S_k = f_k \int s(\rho)\, dL_k, \tag{21}$$

where f_k is a constant for the kth detector which includes the counting efficiency, L_k is path length along the kth chord, and $s(\rho)$ is the source strength in photons/cubic meter.

Assume that the source strength has the form

$$s(\rho) = \sum_j A_j s_j(\rho), \tag{22}$$

where the A_j are constants and the $s_j(\rho)$ are a set of linearly independent functions that can be chosen to suit the purpose, e.g., polynomials such as $s_1 = 1$, $s_2 = \rho$, and $s_3 = \rho^2$, or typical source profile shapes such as $s_1 = (1-\rho^2)$ and $s_2 = (1-\rho^2)^2$. Substituting Eq. (22) into Eq. (21) gives

$$S_k = f_k \sum_j A_j G_{jk}, \tag{23}$$

where

$$G_{jk} \equiv \int s_j(\rho)\, dL_k. \tag{24}$$

Dividing the plasma into a set of nested volume elements whose boundaries are flux surfaces,

$$G_{jk} \simeq \sum_i s_{ij}\, \Delta L_{ik}, \tag{25}$$

where i is summed over all volume elements; s_{ij} is the mean value of $s_j(\rho)$ in the ith volume element; and ΔL_{ik} is the total path length of the kth chord in the ith volume element. The values ΔL_{ik} are obtained by finding the intersections of the

kth chord with the set of flux surfaces as discussed in Section 4 and then simply computing the distance between intersections. For example, for three chords and two source terms we can write the set of equations from Eq. (23) as

$$\begin{pmatrix} G_{11} & G_{21} \\ G_{12} & G_{22} \\ G_{13} & G_{23} \end{pmatrix} \begin{pmatrix} A_1 \\ A_2 \end{pmatrix} = \begin{pmatrix} S_1/f_1 \\ S_2/f_2 \\ S_3/f_3 \end{pmatrix}, \tag{26}$$

which can be solved in a least-squares sense for the A_j. Other treatments are possible. However, in all cases the starting point for the calculation is the determination of the intersections of the chords with a set of nested flux surfaces.

The method described here was used to study the evolution of the plasma density profile in Doublet III [8], although the reference mistakenly refers to the results as "Abel-inverted." The density profile was inferred from the bremsstrahlung source profile, which was computed from bremsstrahlung measurements taken at 1 ms intervals using 15 chords in a fan-shaped array. These chords were lying in the $Z=0$ plane with at least one chord crossing the magnetic axis. The plasma was divided into nine volume elements for the analysis. In this configuration each volume element was intersected by at least one chord, permitting us to solve for a histogram of the source, making no assumptions about the form of the source profile. Formally, we have $s_j(\rho)=\delta_{ij}$ for $\rho_i \leqslant \rho < \rho_{i+1}$, where the ρ_i are the volume element boundaries. Inserting this into Eq. (25) yields $G_{jk}=\Delta L_{jk}$. Then A_j in Eq. (23) is the source strength in the jth volume element and j is summed over the volume elements.

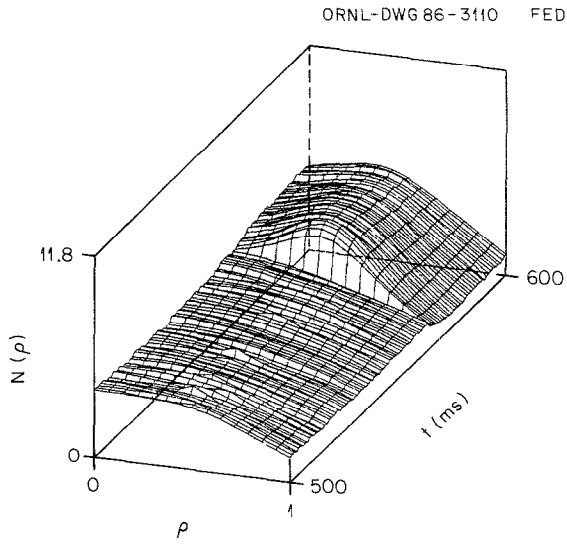

FIG. 8. Time-dependent density profile as inferred from chordal data during pellet injection into Doublet III.

After the histogram of the source was obtained, a 4-parameter fit was made using

$$N(\rho) = N(1) + a_1(1-\rho^2) + a_2 e^{-[(\rho - a_3)/a_4]^2}, \tag{27}$$

where N is the plasma density and the a_m were determined by a least-squares method. This represents a gaussian perturbation to a smooth density profile caused by the injection of a pellet. Figure 8 shows a detail of the results of the calculation. A pellet was injected at about 560 ms. The perturbation broadens slowly as the density diffuses in both directions.

Other forms for the fit were also tried. Reference [8] shows the histogram itself, i.e., the solution for the source profile evolution prior to obtaining a smooth fit. Although the chords in this example all lay in the midplane, in fact the orientation of the chords is arbitrary. The known geometry of the flux surfaces permits a simple solution for the source profile.

6. Concluding Remarks

Spectral representations are currently in use in the data analysis codes of all major tokamak experiments and in many MHD equilibrium codes and tokamak transport codes. The recent emphasis on stellarator experiments is motivating the extension of existing two-dimensional techniques to more general geometries. The algorithms described here are fully three dimensional and can be adapted easily to alternate definitions of the flux coordinates.

The authors will furnish a suite of FORTRAN subroutines containing these algorithms to interested parties. These routines have been tested and used in analysis of tokamak data from Doublet III and stellarator data from Heliotron E. Parts of the code are in use for transport simulation at Oak Ridge and Princeton. However, those people preferring to write or modify their own code should find that the algorithms are complete as described and that the programming effort required is not excessive.

References

1. S. P. Hirshman and J. C. Whitson, *Phys. Fluids* **26** (12), 3553 (1983).
2. A. Bhattacharjee, J. C. Wiley, and R. L. Dewar, *Comput. Phys. Commun.* **31**, 213 (1984).
3. L. Lao, *Comput. Phys. Commun.* **31**, 201 (1984).
4. U. Schwenn, *Comput. Phys. Commun.* **31**, 167 (1984).
5. M. D. Kruskal and R. M. Kulsrud, *Phys. Fluids* **1**, 265 (1958).
6. S. Hamada, *Nucl. Fusion* **1**, 23 (1962).
7. R. S. Granetz and J. F. Camacho, *Nucl. Fus.* **25** (6), 727 (1985).
8. S. Sengoku *et al.*, *Nucl. Fus.* **25** (10), 1475 (1985).
9. C. O. Beasley, J. A. Rome, S. E. Attenberger, and S. P. Hirshman, Oak Ridge National Laboratory/Technical Memo-10222, 1986 (unpublished).
10. S. P. Hirshman, K. C. Shaing, W. I. van Rij, C. O. Beasley, Jr., and E. C. Crume, Jr., *Phys. Fluids* **29** (9), 2951 (1986).
11. G. E. Forsythe, M. A. Malcolm, and C. B. Moler, *Computer Methods for Mathematical Computations* (Prentice–Hall, Englewood Cliffs, NJ, 1977), p. 161.